

RESEARCH

Open Access



# The high impact of zinc chromium oxide nanocombs on development of larvicidal and antimicrobial performance

Wageha A. Mostafa<sup>1</sup>, Soad A. Elshanawany<sup>2</sup>, Khadejah D. Otai<sup>3</sup>, Mona khalifa<sup>4</sup> and Elsayed Elgazzar<sup>5\*</sup>

## Abstract

Zinc chromium oxide (Cr/ZnO, 5wt.%) was prepared by a facile chemical co-precipitation route. The structure, composition, and chemical bonding were analyzed using X-ray diffraction (XRD), Energy dispersive X-ray spectroscopy (EDX), and Fourier-transform infrared spectroscopy (FTIR) indicating that chromium ions were integrated the host framework to form Cr/ZnO nanocomposite. Scanning electron microscopy (SEM) and Transmission electron microscopy (TEM) micrographs showed comb-shaped nanoparticles with an average size 20 nm and large surface area. The energy gap of the thin films was estimated from T% and R% measurements which exhibit a strong optical absorption edge close to the visible spectrum. The insecticidal activity of the synthesized nanocombs against *C. pipiens* larvae was evaluated with LC<sub>50</sub> (30.15 ppm) and LC<sub>90</sub> (100.22 ppm). Besides, the nanocomposite showed high antibacterial performance against gram-positive bacteria (*Bacillus subtilis*) and gram-negative bacteria (*Proteus vulgaris*) with inhibition zones 21.9 and 19 mm, respectively.

**Keywords** Cr/ZnO nanocombs, Energy gap, Larvicidal, Ultrastructure alteration, Bactericidal

## Introduction

Global warming causes climate variation which is the essential factor in the spread of climate-sensitive infectious [1]. A temperature rise enhances vector and pathogen metabolism allowing faster prevalence, whereas unpredictable rainfall patterns may exceed the availability of favorable breeding sites [2, 3]. The combination of warm and moderate humidity provides typical conditions

for several types of species *Aedes*, *Culex*, and *Anopheles* mosquitoes to survive transferring diseases like dengue, filariasis, yellow fever, and zika virus [4, 5]. For instance, lymphatic filariasis and West Nile fever are mainly vectored by *Culex pipiens*. Additionally, controlling mosquito vectors carries several dangers due to the vector resistance to conventional pesticides as well as their negative impact on the environment and human health [6, 7]. On the other side, microorganisms including bacteria, fungi, and protozoa pose a great danger to individuals, animals, and plants. World Health Organization (WHO) states that the rapid emergence of infectious diseases owing to infectious bacteria threatens all the world's countries causing millions of deaths annually [8]. Biofilm formation by pathogens in bacterial communities such as multicellular organisms show significant resistance to antibiotics leading to health and economic problems especially in poor countries because of the high therapy costs [9]. Taking these risks seriously, there is an urgent

\*Correspondence:

Elsayed Elgazzar

elsayed.elgazzar@yahoo.com; elsayed\_mohsen@science.suez.edu.eg

<sup>1</sup> Entomology Section, Zoology Department, Faculty of Science, Zagazig University, Zagazig, Egypt

<sup>2</sup> Physics Department, Jazan University, 86736 Jazan, Saudi Arabia

<sup>3</sup> Department of Chemistry, Samtah University College, Jazan University, 86736 Jazan, Saudi Arabia

<sup>4</sup> Biochemistry department, Faculty of Science, Cairo University, Cairo, Egypt

<sup>5</sup> Department of Physics, Faculty of Science, Suez Canal University, Ismailia 41522, Egypt



© The Author(s) 2024. **Open Access** This article is licensed under a Creative Commons Attribution 4.0 International License, which permits use, sharing, adaptation, distribution and reproduction in any medium or format, as long as you give appropriate credit to the original author(s) and the source, provide a link to the Creative Commons licence, and indicate if changes were made. The images or other third party material in this article are included in the article's Creative Commons licence, unless indicated otherwise in a credit line to the material. If material is not included in the article's Creative Commons licence and your intended use is not permitted by statutory regulation or exceeds the permitted use, you will need to obtain permission directly from the copyright holder. To view a copy of this licence, visit <http://creativecommons.org/licenses/by/4.0/>. The Creative Commons Public Domain Dedication waiver (<http://creativecommons.org/publicdomain/zero/1.0/>) applies to the data made available in this article, unless otherwise stated in a credit line to the data.

need to uncover economical, biocompatible, competitive, and effective alternative methods to replace traditional treatments.

Nanomaterials have emerged as strong antimicrobial and larvicidal agents depending on their quantum size effect, large surface area to volume ratio, and high chemical reactivity. Metal and metal oxide nanoparticles (NPs) have been applied in various fields comprising medicine, drug delivery, energy, agricultural, catalysis, and biosensors [10]. For example, zinc oxide (ZnO), magnesium oxide (MgO), tin oxide (SnO<sub>2</sub>), silver oxide (Ag<sub>2</sub>O), zirconium oxide (ZrO<sub>2</sub>) and copper oxide (CuO) have been utilized as highly efficient nanomaterials in health care sector [11–13]. In particular, ZnO NPs have drawn much attention as an antimicrobial and anticancer agent for inhibiting the microorganism's growth thanks to their semiconducting nature, safety, and unique physicochemical characteristics. Recent studies have reported the capability to modify the microstructure of nanomaterial by doping for enhancement of its physical and chemical properties. Integration of the ZnO matrix with different metal ions; Mn, Fe, Cr, Ag, Cu, Cd, Sn, Ga, etc., will create intermediate energy levels and hence increase free charge carriers' mobility [13, 14]. Tuan Vu et al. have developed gold/zinc oxide (Au/ZnO) nanoflower as a strong photocatalyst and an antimicrobial agent for the degradation of Tartrazine (TA) and killing *Escherichia coli* (E. coli) [15]. Also, Abd El-Latef et al. have substituted Cu<sup>2+</sup> into ZnO matrix by hydrothermal assisted co-precipitation method for enhancement of insecticidal activity against *Spodoptera littoralis* [16]. Among various transition metals, chromium is a promising dopant owing to the close ionic radius of Cr<sup>3+</sup> (0.063 nm) to Zn<sup>2+</sup> (0.074 nm); besides, the electronegativity of Zn is similar to Cr ~ 1.66. Moreover, chromium oxide (Cr<sub>2</sub>O<sub>3</sub>) is a p-type with an energy gap of 3.10 eV which is useful for increasing active sites and oxygen species [17, 18]. In this context, Shah et al. have prepared ZnO and chromium doped ZnO nanoparticles using leaf extract of *Citrus reticulata* indicating strong biological activities against *E. coli*, *S. aureus*, *K. pneumonia* and *P. aeruginosa* with zone of inhibition of 22.4 ± 1.98, 15.5 ± 0.78, 10.2 ± 0.55 and 7.5 ± 1.55 mm, respectively dependence of high generation of reactive oxygen species [19]. In medical applications, Cr doped ZnO has been applied as a therapy for estimating the cytotoxic effects using human fetal lung fibroblast cells (WI38 cells) based on the morphological nature of the nanoparticles [20]. To date, several techniques are employed for fabricating nanoscale materials including hydrothermal, co-precipitation, chemical vapor deposition, spray pyrolysis, solution combustion, sol-gel, and magnetron sputtering. Among them, a simple, scalable, and controllable chemical co-precipitation technique was

performed to obtain high quality nanoparticles [20, 21]. The current work aims to modify the topological nature of ZnO NPs by Cr<sup>3+</sup> replacements to one dimensional nanocomb structure for biomedical applications.

## Experimental section

### Chemicals and reagents

Zinc chloride dihydrate, ZnCl<sub>2</sub>·2H<sub>2</sub>O, 98.0%, Sodium hydroxide (NaOH ≥ 98.0%), Chromium nitrate nonahydrate Cr(NO<sub>3</sub>)<sub>3</sub>·9H<sub>2</sub>O, ≥ 97.0%), Cacodylate buffer, Glutaraldehyde, Osmium tetroxide (OsO<sub>4</sub>), Ethanol, and Acetone were purchased from Alfa Aesar, All reagents were used without any purification,

### Preparation and characterization of zinc chromium oxide nanocomposite

Zn<sub>x</sub>Cr<sub>1-x</sub>O, x = 5 wt% was prepared by chemical co-precipitation approach. Firstly, 8.35 g zinc chloride dihydrate was dissolved in 50 ml double distilled water and 1.28 g chromium nitrate nonahydrate in 25 ml under a magnetic stirrer. Chromium salt solution was carefully added to zinc chloride with continuous stirring for 3h at room temperature. 2.92 g sodium hydroxide (NaOH) was dissolved in 65 ml double distilled water and then slowly added drop by drop to aqueous solutions under stirring at a constant speed for 4h without heating. A homogeneous white gray precipitate was formed at pH ~ 9. Then separated using filter paper and washed many times with distilled water. The resulting powder was dried in a furnace at 70 °C overnight and eventually annealed at 400 °C for 2h.

### Characterization of the nanomaterial

The phase and crystallographic features of Cr/ZnO nanocomposite were recognized by XRD (Bruker D8 Advance Eco) operated at λ = 1.54 Å (Cu Kα radiation) at 2θ angle varied from 25° to 75°. Morphological nature and elemental composition were recorded using scanning electron micrograph (SEM; Helios Nanolab. 400) attached with energy dispersive X-ray analysis (EDX). The functional group was identified by Fourier transform infrared (FT-IR spectrum 100, Perkin Elmer) at a resolution of 400–2000 cm<sup>-1</sup> with 16 scan speed. Transmission electron microscopy (TEM; Model: JEOL JEM-2100) was carried out to visualize the average size and particle's shape. A spin coater sputter coater (Model, EMS 150T ES) was utilized to fabricate the thin films. Transmittance (T%) and reflectance (R%) spectra were measured via UV-Vis spectrophotometer JASCO (V-570) to investigate the energy gap of the fabricated thin films.

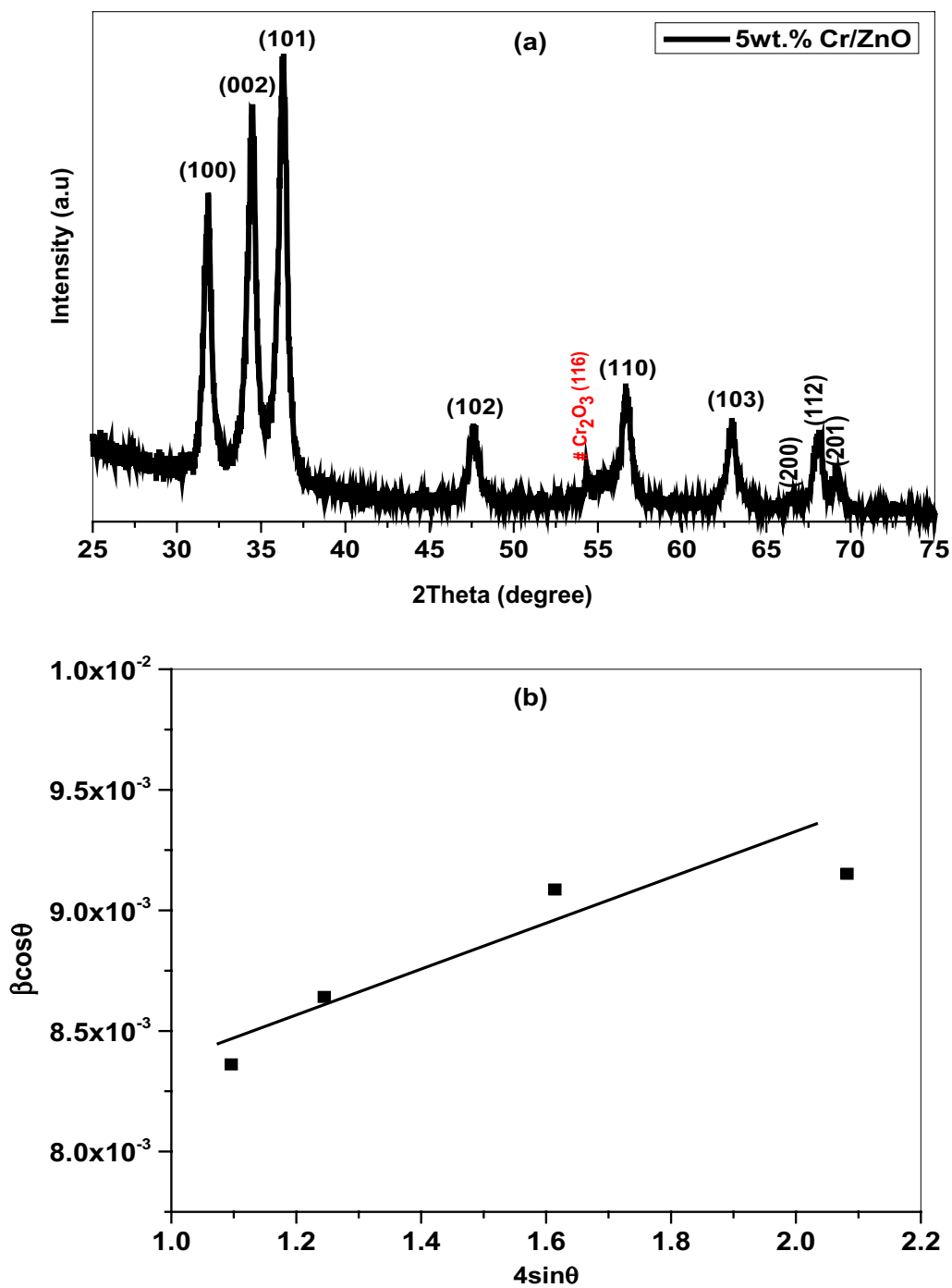
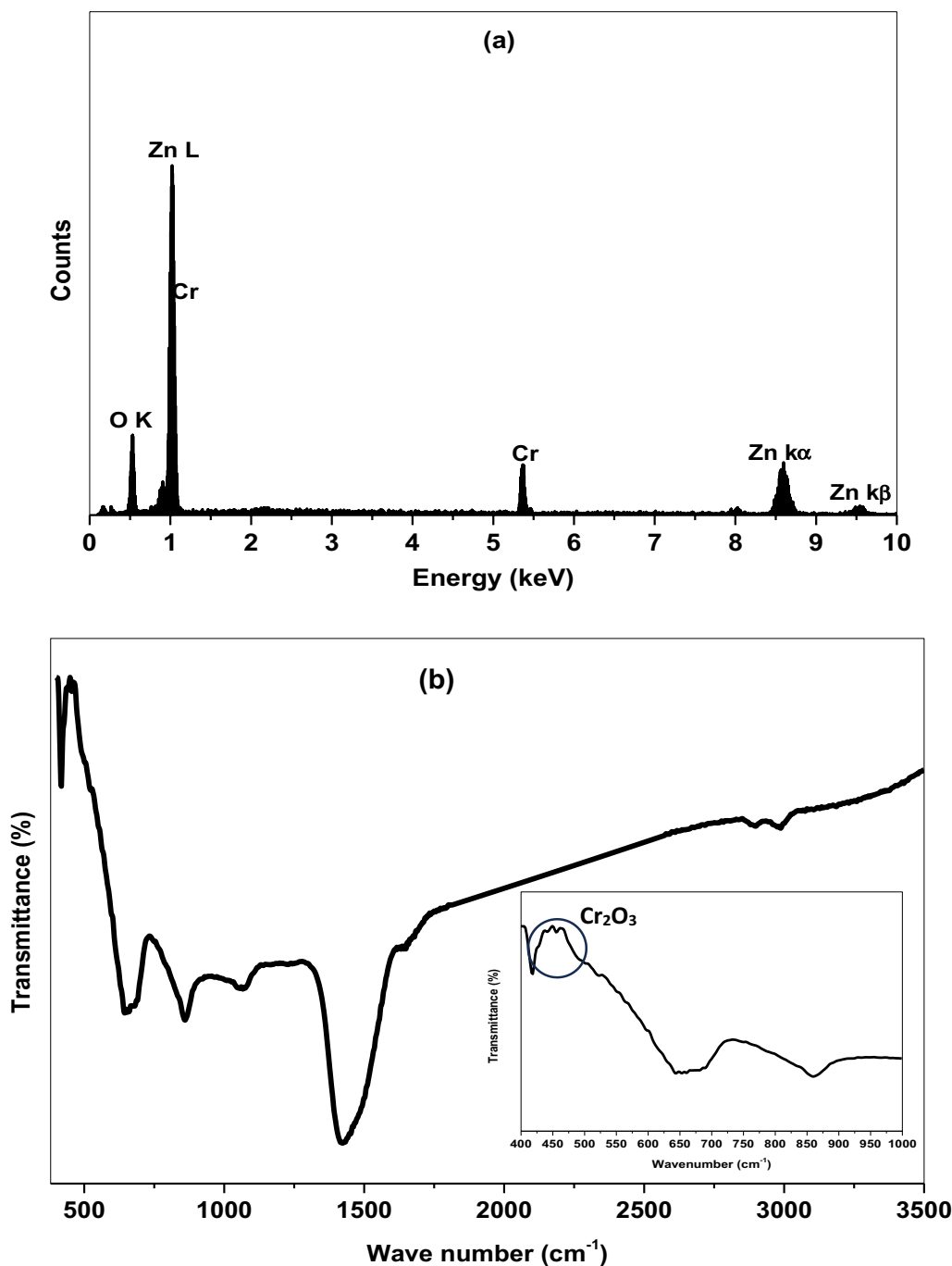


Fig. 1 a XRD pattern and b W–H plot of Cr/ZnO nanocomposite

**Table 1** Crystallographic parameters of Cr doped ZnO nanocomb obtained from W–H plot and Scherrer formula

Crystallographic parameters						
W–H plot			Scherrer equation			
Nanocomb	D(nm)	$\epsilon \times 10^{-4}$	D(nm)	$\epsilon \times 10^{-4}$	$\delta \times 10^{-4} \text{nm}^{-2}$	$X_c$
Cr/ZnO	18.97	7.84	16.74	69.00	35.70	26.73



**Fig. 2** a EDX spectrum and b FTIR of Cr/ZnO nanocomposite

**Mosquito rearing**

The egg rafts of *C. pipiens* were kept and hatched at a controlled temperature of 27 – 30° and 80% humidity. The larvae fed on fish food and grew in plastic trays that measured 30 × 25 × 5 cm. As for the adult mosquitoes, they were kept in cages that measured 30 × 30 × 30 cm and fed with a solution that contained 10% glucose.

**Larvicidal activity**

The insecticidal activity was investigated by placing 25 mosquito larvae into 200 mL of sterilized double-distilled water with Cr/ZnO at concentrations (25, 50, 100, 150, and 200 ppm) in a 250 mL beaker. Pure water was applied as a control for each individual concentration. The dead larvae were recorded after 24h of treatment,

and the death percentage was calculated from the average of replicates [22]. Further, this formula was used to determine the fatal rates.

$$\text{Mortality (\%)} = \frac{(\text{No. of dead larvae})}{(\text{total of larvae introduced})} \times 100 \quad (1)$$

#### Ultrastructure examination

The midgut ultra-structural alteration of *C. pipiens* larvae was investigated after exposure to Cr/ZnO NPs according to El-Samad et al. with a little modification [23] and the tissues were examined with a JEOL 1200 EX II transmission electron microscope at the central laboratory, Faculty of Science, Zagazig University.

#### Antibacterial activity

The antibacterial performance of the prepared specimen was investigated by the disc diffusion method against pathogenic bacteria such as *Staphylococcus aureus*, *Bacillus subtilis* and *Bacillus cereus* (gram-positive), and *Escherichia coli*, *Proteus vulgaris* and *Pseudomonas aeruginosa* (gram-negative). Whatman No.1 filter paper discs of 6 mm dia. were immersed with 10 and 30  $\mu\text{g}$  of Cr/ZnO NPs synthesized nanocomposites for each strain and determined the zones of inhibition around the disks after incubating the plates at 37 °C for 24 h [24]. Each examination was repeated three times, then the data were analyzed using statistical methods and using Gentamycin (4  $\mu\text{g}/\text{ml}$ ) as a positive control of bacteria. All findings were statistically calculated as the mean  $\pm$  standard error (SE) of the average values. The

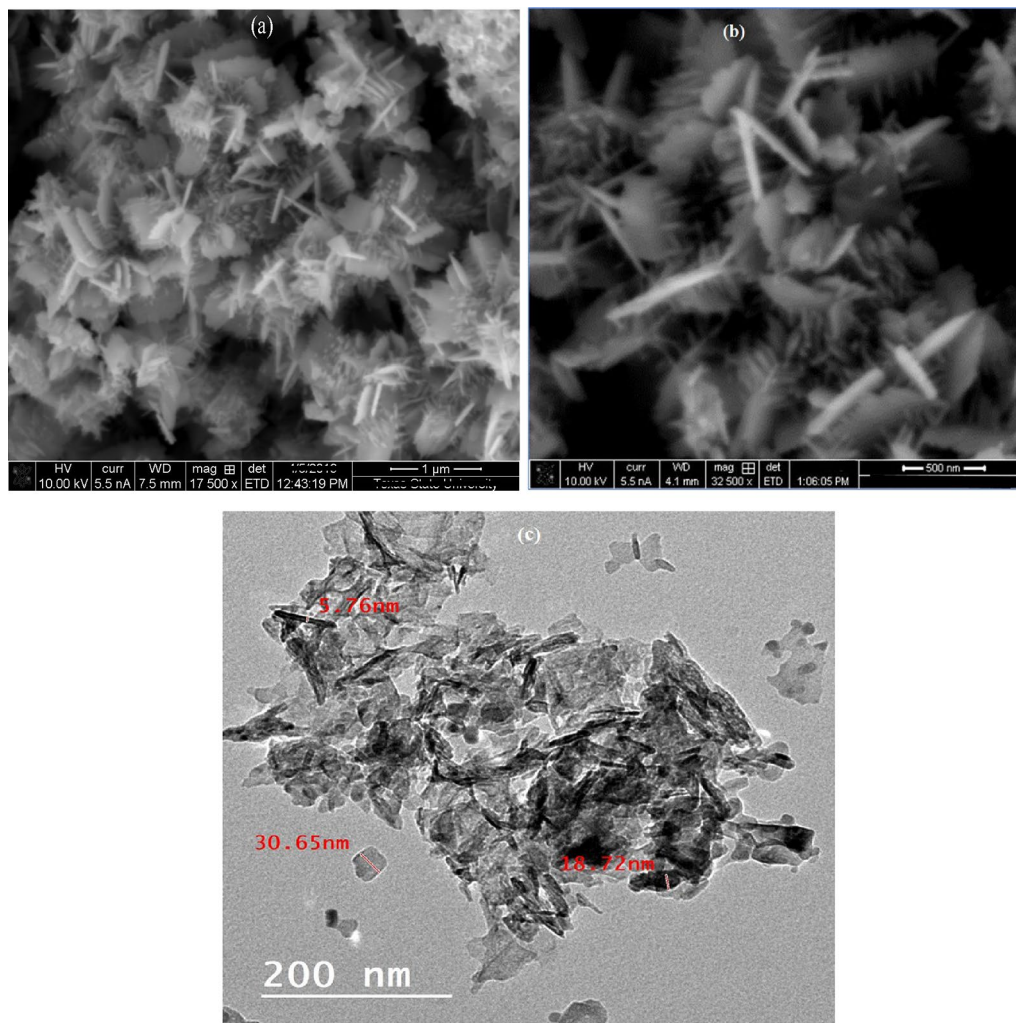


**Fig. 3** a, b SEM micrograph and c TEM micrograph of Cr/ZnO nanocomb

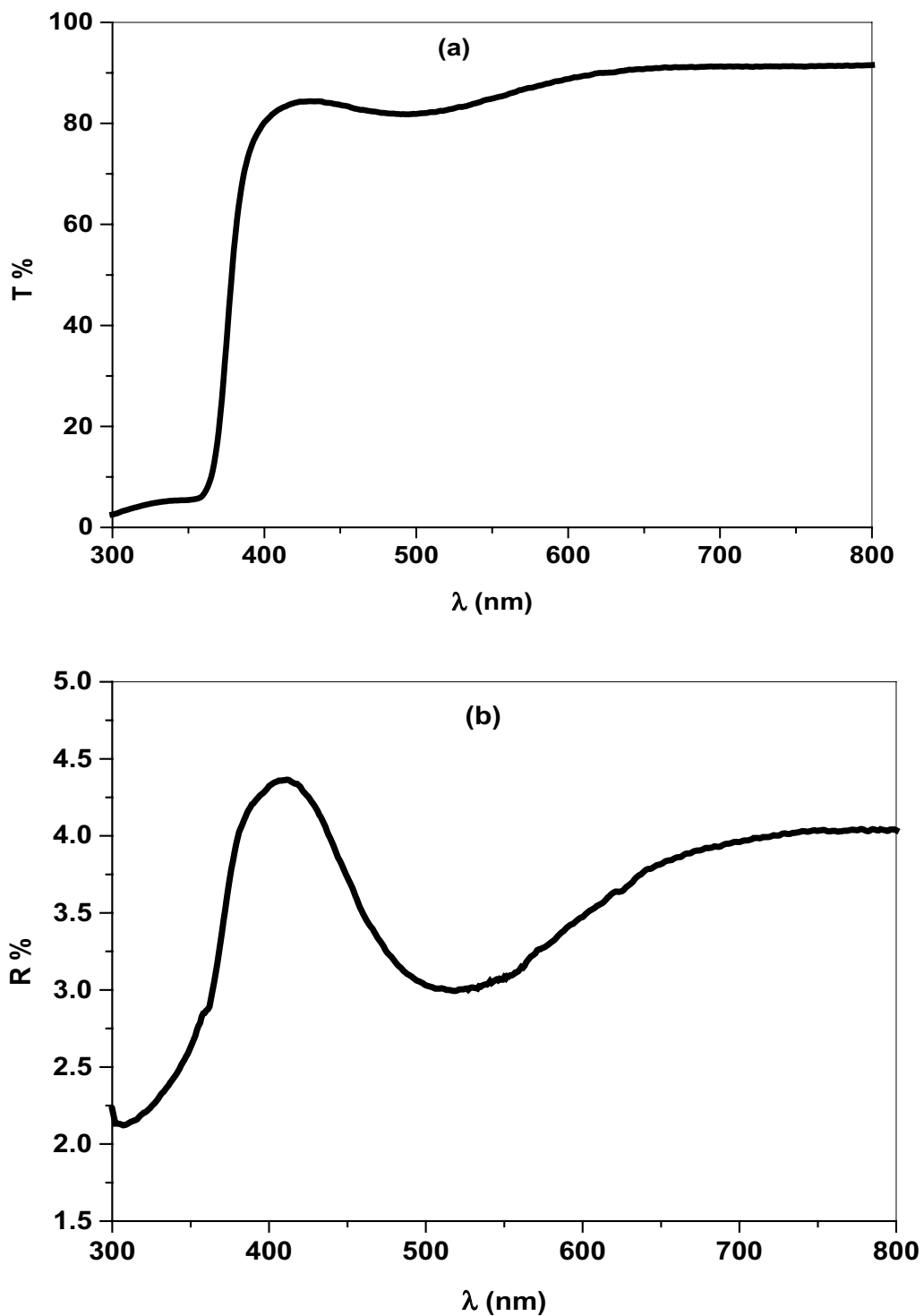
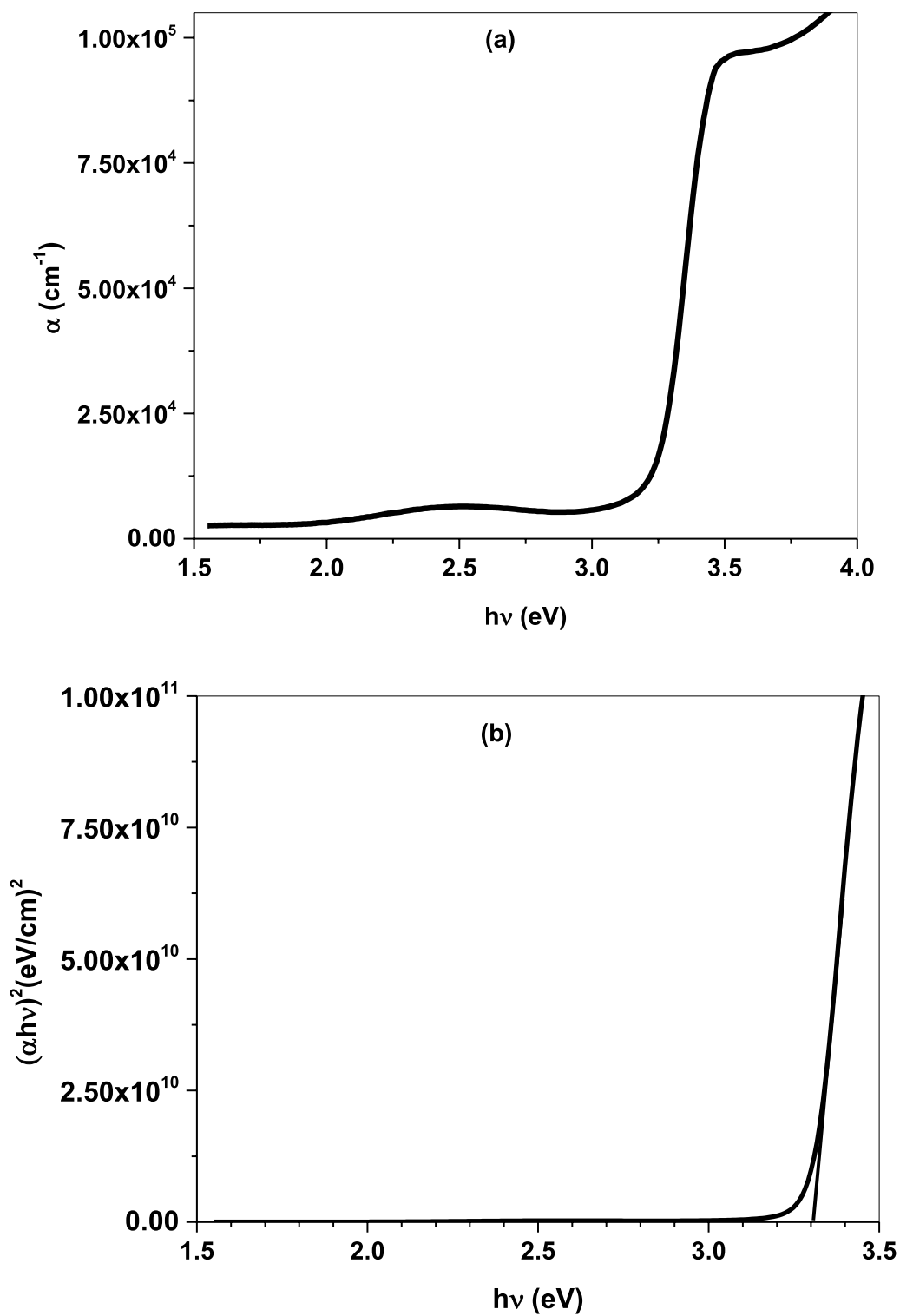


Fig. 4 a Optical transmittance and b Reflectance of Cr/ZnO thin film



**Fig. 5** a Optical absorption and b Energy gap of Cr/ZnO thin film

**Table 2** Toxic effect of nanostructure Cr/ZnO against third larval instar of *C. pipiens*

Concentrations (ppm)	Mean $\pm$ S.E	LC <sub>50</sub> (LCL)	LC <sub>90</sub> (UCL)	Regression equation	X <sup>2</sup>
25	35 $\pm$ 0.629 <sup>a</sup>				
50	73.75 $\pm$ 0.47 <sup>ab</sup>	30.15	100.22	Y = -4.07 + (X $\times$ 1.19)	9.7
100	80 $\pm$ 0.64 <sup>b</sup>	(24.12: 35.71)	(82.55:131.66)		
150	92.5 $\pm$ 0.288 <sup>c</sup>				
200	100 $\pm$ 0.00 <sup>d</sup>				

LC<sub>50</sub> and LC<sub>90</sub>: lethal concentration that kills 50 and 90% of the exposed *C. pipiens* larvae; UCL: upper confidence limit; LCL: lower confidence limit; X<sup>2</sup> = Chi-square, p < 0.05, significance level, Mean value of five replicates, (SE) standard error. Control (distilled water), nil mortality. Letters indicate degree of significant based on Tukey's HSD tests between different treatments and control. Letter (a) mean high significant, and letter (c) mean low significant, while the same letters are not significantly different

chi-square method was utilized to show the significant difference, the obtained data was compared with the control group using regression co-efficient. Also, Probit transformation analysis was applied to determine the LC<sub>50</sub> and LC<sub>90</sub> values.

## Results and discussion

### Structural analysis

The XRD profile of Cr/ZnO nanostructures was illustrated in Fig. 1a. As can be seen, the prepared nanopowder of polycrystalline nature and well-defined peaks located at 31.85°, 34.49°, 36.30°, 47.72°, 56.79°, 62.98°,

66.59°, 68.17°, 69.24° corresponding to the reflection planes 100, 002, 101, 102, 110, 103, 200, 112, 201 ascribed to the hexagonal wurtzite structure and coincide with the standard card JCPDS No. 36-1451, space group (P63mc). The sample has a relatively intense peak however the observed broadening clearly reveals the small crystal size of the nanocomposite. No phases related to impurities or unreacted ions were observed in the pattern, otherwise the weak peak located at  $2\theta = 54.25^\circ$  is attributed to chromium oxide (Cr<sub>2</sub>O<sub>3</sub>). Despite the close ionic radius of Cr<sup>3+</sup> to Zn<sup>2+</sup>, the large amount of chromium ions concentrations (Cr<sup>3+</sup>, 5 wt.%) inside the host framework led to phase segregation [25–27]. Moreover,

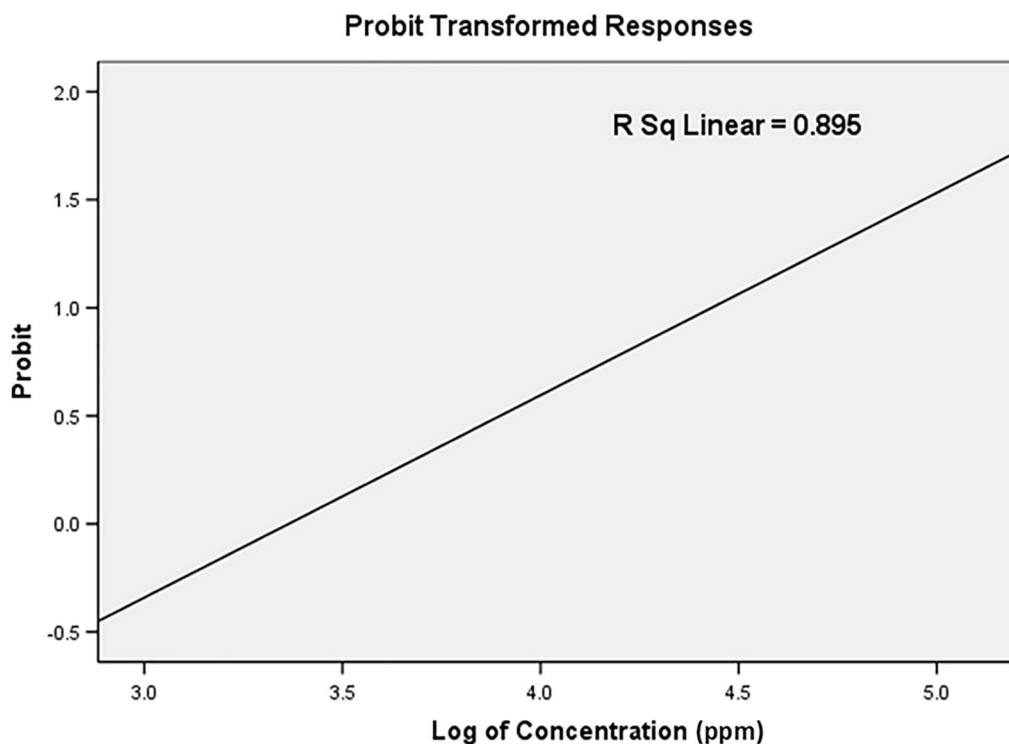


**Fig. 6** The probability analysis of mortality of *C. pipiens* mosquito larvae exposed to Cr/ZnO nanocomb

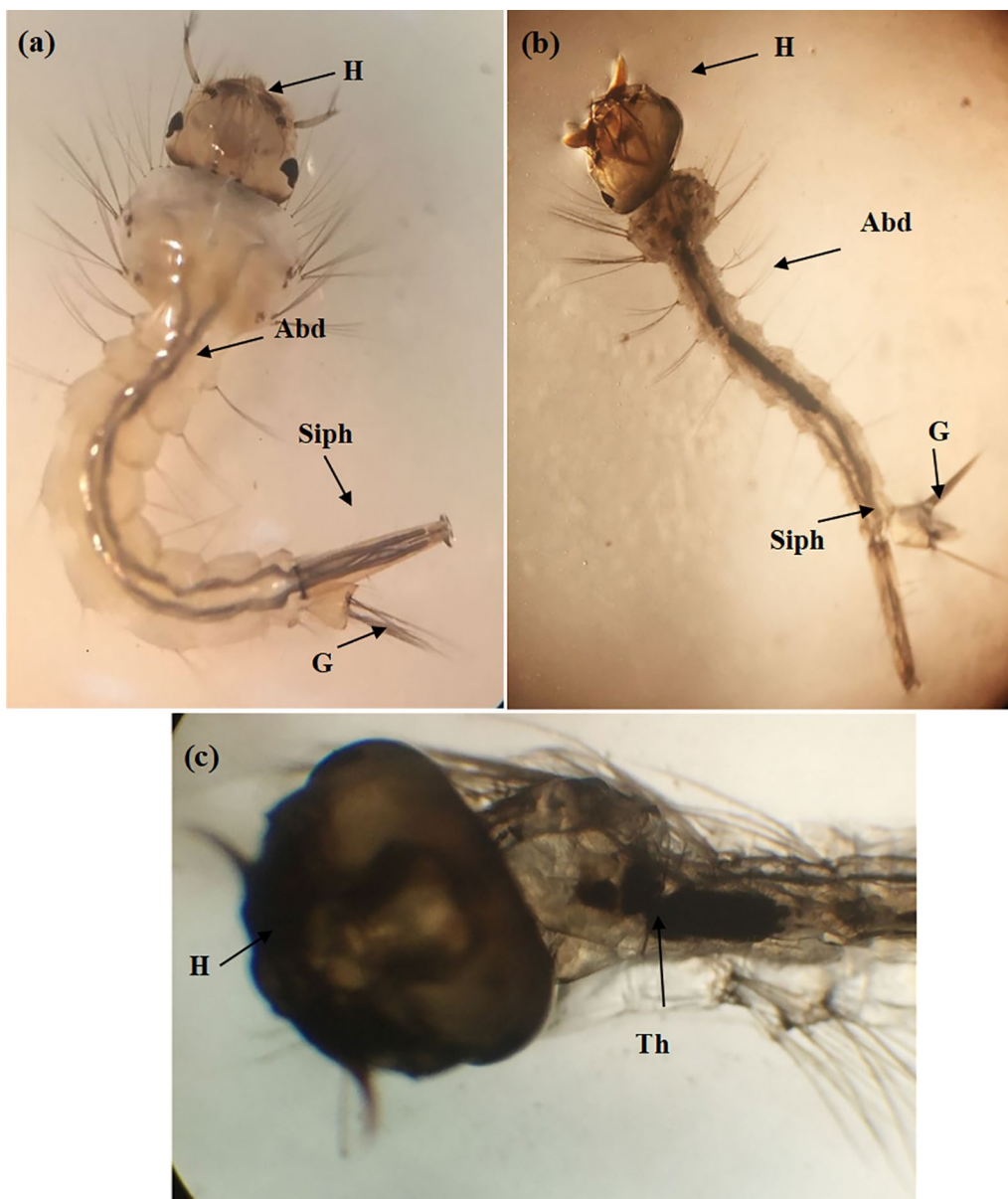


**Fig.7** Light microscope photographs of body parts (head, abdomen, and respiratory opening) of the 3rd larval instars of *Cx. pipiens* control **a** and larvae treated with Cr/ZnO NPs **b, c** (10×40) (Abd: abdomen; G: gills; H: head; Siph: siphon; Th; thorax)

the crystallographic parameters including crystalline size (D) and lattice strain (ε) were determined from the Williamson-Hall (W-H) plot expressed as:

$$\beta \cos\theta = \frac{k\lambda}{D} + 4\epsilon \sin\theta \tag{2}$$

where, β is the full width at half maximum (FWHM), θ is the Bragg’s diffraction angle, λ is the X-ray wavelength = 1.5418 Å, and k is a constant = 0.94. The internal strain was given from the slope and the crystallite size was defined from the intercept =  $\frac{k\lambda}{D}$ , Fig. 1b. Scherrer

equation was also applied to evaluate the size of crystals by the following equation:

$$D = \frac{K\lambda}{\beta \cos\theta} \tag{3}$$

Lattice strain (ε), dislocation density (δ) and degree of crystallinity (X<sub>c</sub>) were estimated by the formulas:

$\epsilon = \frac{\beta}{4 \tan\theta}$ ,  $\delta = \frac{1}{D^2}$ , and  $X_c = \frac{0.24}{\beta}$ , respectively. As presented in Table 1, the nanocomposite shows a crystallite size range from 17–19 nm. In addition to, large strain

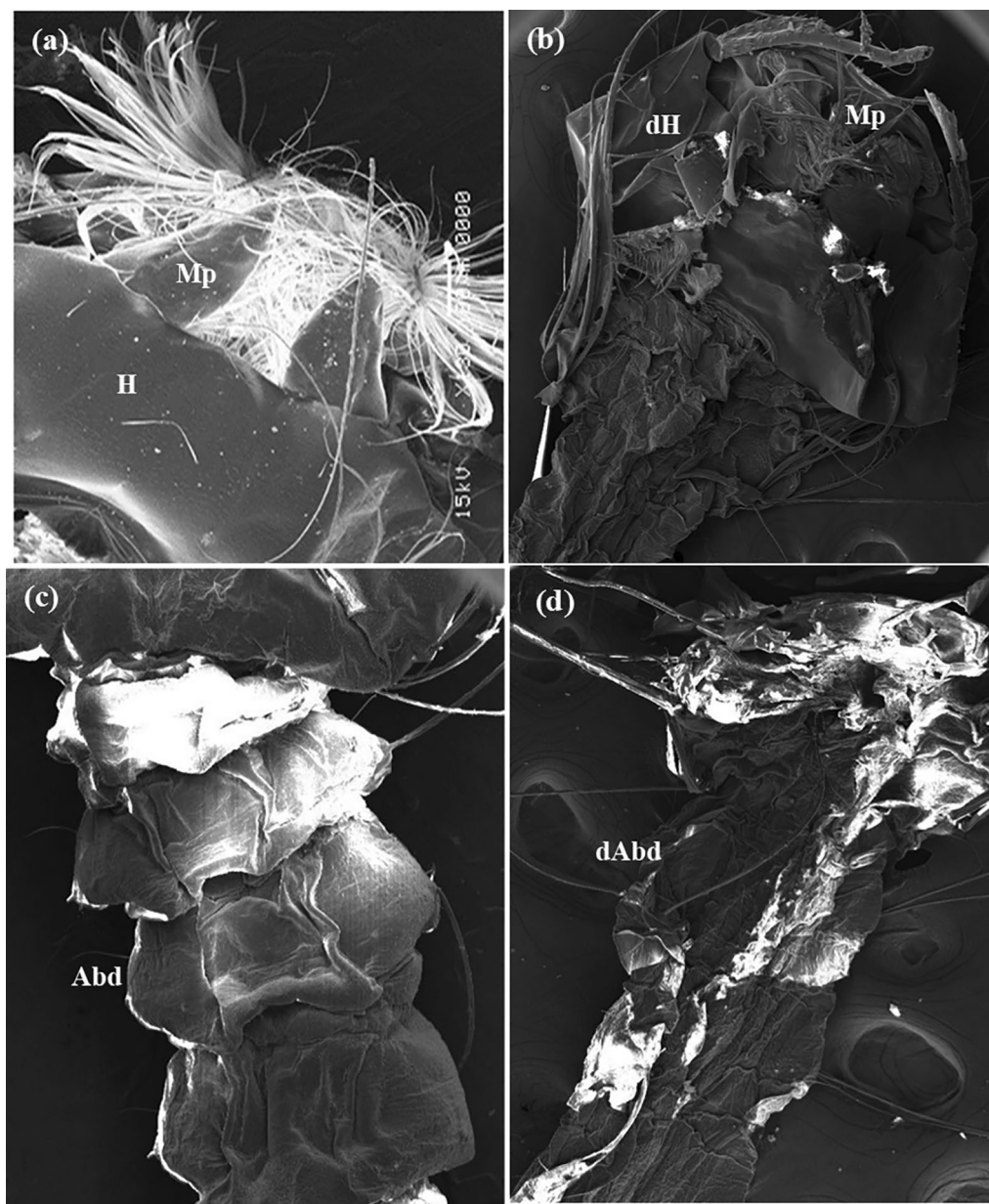


**Fig. 8** The SEM micrographs of third larval instar of control *C. pipiens* larvae **a, c** showed normal head capsule, mouth parts and abdominal segments, **b, d** larvae treated by Cr/ZnO NPs at 48 h post treatment showed deformed head capsule, mouth parts and abdominal segments (*Abd* abdomen, *dAbd* deformed abdominal segments, *H* head; *dH*: deformed head; *Mp*; mouthparts)

and dislocation density associated with the presence of Cr contents and crystal defects that prevented the crystal growth result in crystal size reduction [27, 28].

#### Composition and functional group identification

The chemical composition and purity of Cr/ZnO NPs were investigated from EDX spectroscopy. The spectrum has detected the compositional peaks of Zn, O,

Cr elements of weight percentages (wt.%) 62.16, 29.72, and 8.12 respectively. The presence of chromium peak in EDX spectrum reveals the incorporation of  $\text{Cr}^{3+}$  into the host matrix, Fig. 2a [29, 30]. The absence of impurities related to unreacted ions emphasizes the high purity of the nanocomposite. The functional group and chemical bonding were defined from FTIR through wavenumber range from 400 to 3500  $\text{cm}^{-1}$  as depicted in Fig. 2b.

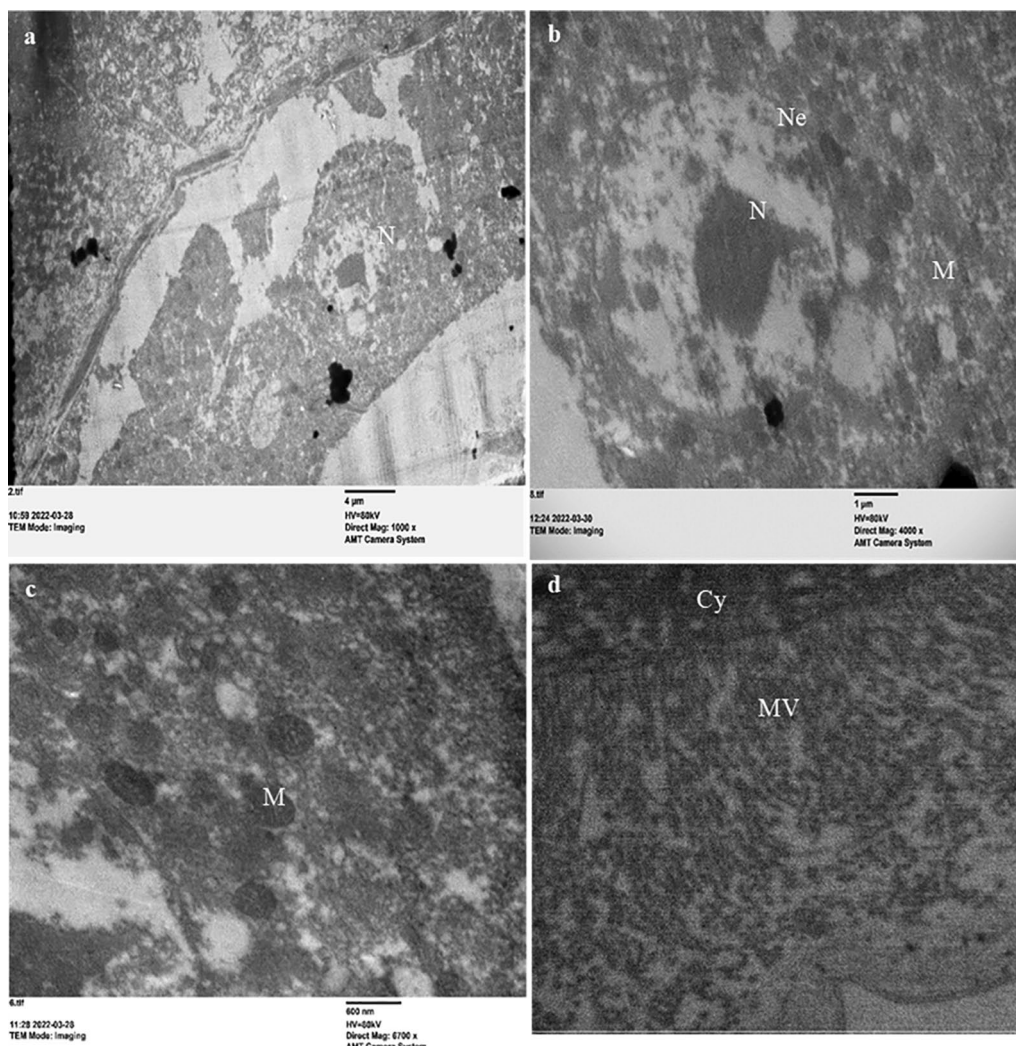


**Fig. 9** Transmission electron micrographs showing the ultrastructural in the midgut of the normal third larval instar of *C. pipiens* mosquito **a, b** The normal structure of the epithelium showing the nucleus having scattered chromatin. **c, d** the gut cytoplasm has mitochondria and microvilli. Cy(cytoplasm), M (mitochondria), N (nucleus), Ne (nuclear envelope), and MV (microvilli)

The vibrational bands at  $729.43\text{ cm}^{-1}$  and  $860.52\text{ cm}^{-1}$  are attributed to the stretching mode the Zn – O bond. Besides, the weak absorption bands at  $438.40\text{ cm}^{-1}$  is assigned to chromium oxide ( $\text{Cr}_2\text{O}_3$ ). The two weak bands at  $447.67\text{ cm}^{-1}$  and  $462.23\text{ cm}^{-1}$  are associated with metal oxide Zn – O – Cr and Cr – O bonds, respectively. In general, nanometal oxides exhibit vibrational frequencies at wavenumber less than  $1000\text{ cm}^{-1}$ . The observed weak IR bands at wavenumber varied between  $1265$  and  $1470\text{ cm}^{-1}$  are assigned to O-H stretching vibrations which arises from absorbing atmospheric moisture [31, 32]. The FTIR spectrum clearly approves that chromium ions have occupied zinc oxide framework as demonstrated in the XRD result.

### Morphological characteristics

The surface morphology of the synthesized nanocomposite was visualized by SEM micrograph executed at different magnifications. As described in Fig. 3(a,b), the particles appear in nanocomb-like shapes, aggregated together with high density. The surface appears not uniform and has different shapes; some particles take thin flake shape [33]. Sharp needles linked to nanocomb were observed in the SEM image, Fig. 3b. These needles have a strong impact on killing microbes and mosquitoes. Further, average size and particles distribution were determined by TEM micrograph. Figure 3c, shows the particles in thin sheet, needle, and spherical shape with mean size  $\sim 20\text{ nm}$ . Little needles are assembled in nanorods

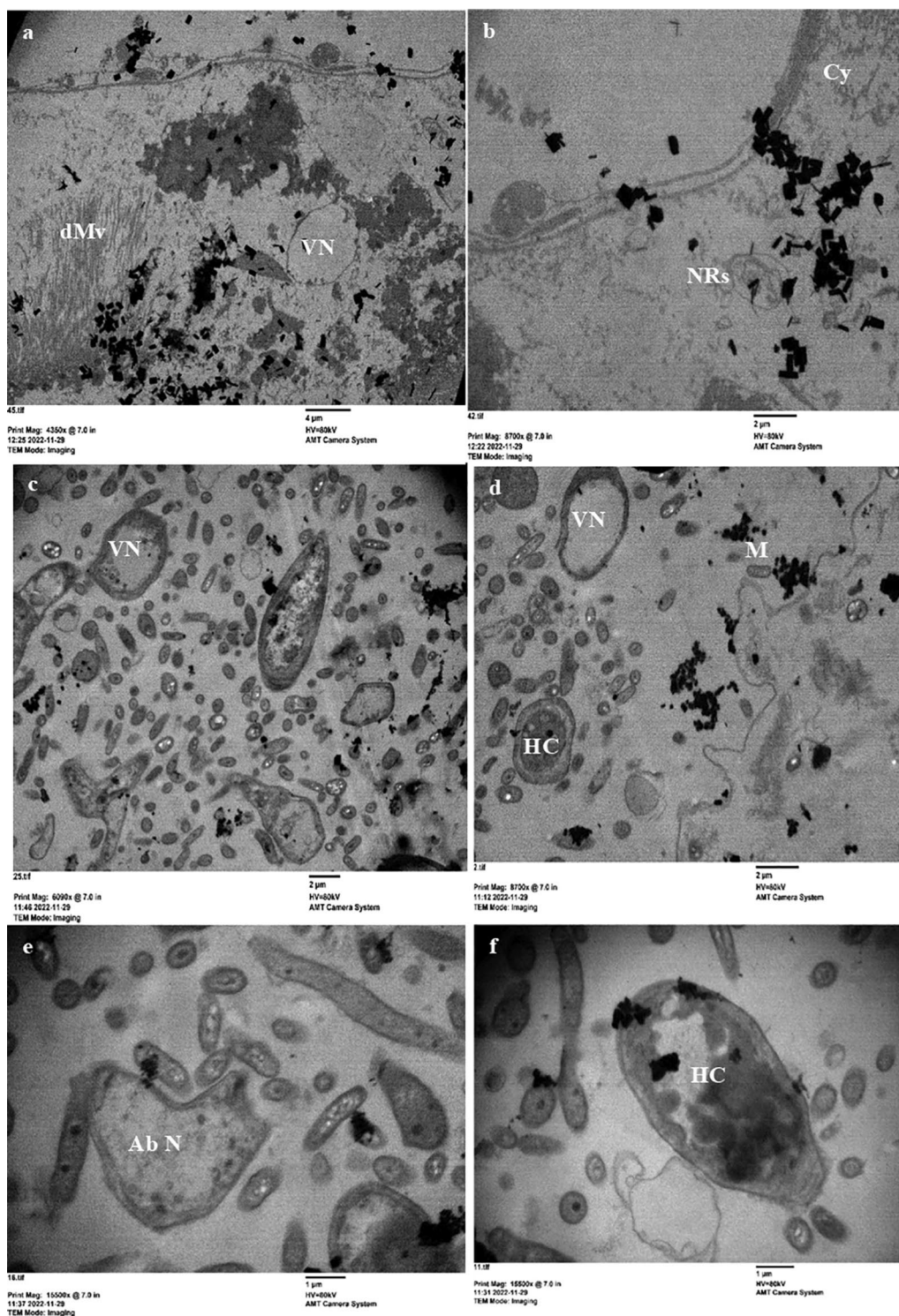


**Fig. 10** Transmission electron micrographs showing the ultrastructural changes in the midgut of the third larval instar of *C. pipiens* mosquito in response to LC<sub>50</sub> treatment with Cr/ZnO NPs **a, b** An epithelial cell in treated larvae showing missed microvilli and clear condensation of the nucleus with clear vacuolation in the cytoplasm near the basement membrane. **c, d** the cells have vacuolated nuclei and nucleus with heterochromatin. **e, f** The epithelium in the treated larva vacuolated and have abnormal nucleus shapes. Cy (cytoplasm), dMV (microvilli), HC (heterochromatin), M (mitochondria), Ab N (abnormal nucleus) and VN (vacuole nucleus)

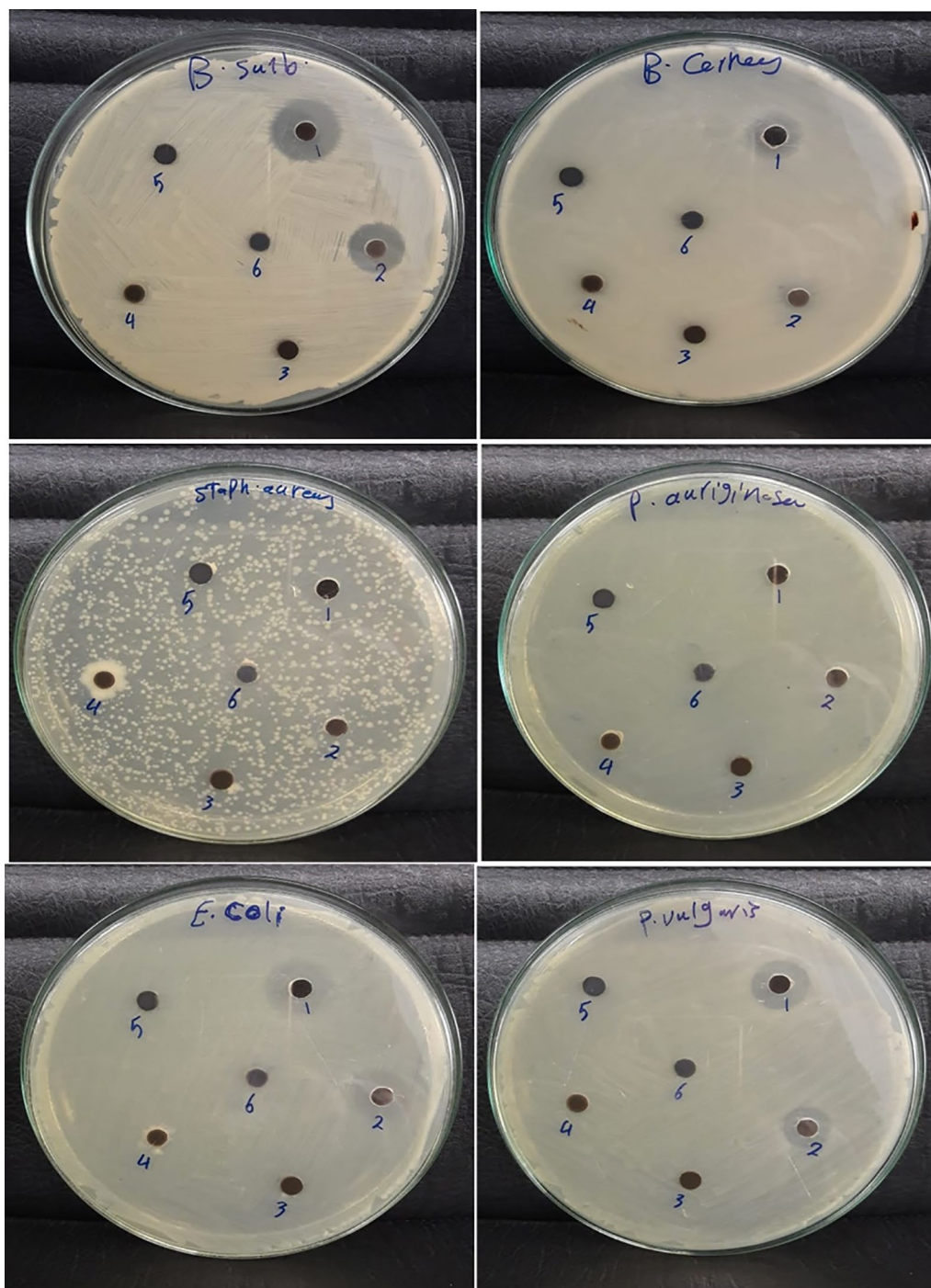


**Fig. 11** The inhibition zones indicating the antimicrobial activity of Cr/ZnO against gram positive and gram-negative bacteria

of diameter  $\sim 6$  nm, length 80 nm, and aspect ratio  $\sim 13$  [34, 35]. The microstructure analysis has approved that the nanocombs possess superior architecture topological features. Where, the dimensions confinement and small size enable them to be used as antimicrobial and larvicidal agent for human health protection.

**Optical analysis**

The optical characteristics of Cr/ZnO coated thin film were analyzed from transmittance (T%) and reflectance (R%) spectra through the wavelength varied between 300 – 800 nm. The thin film exhibited high optical transmittance greater than 82% in the visible region.

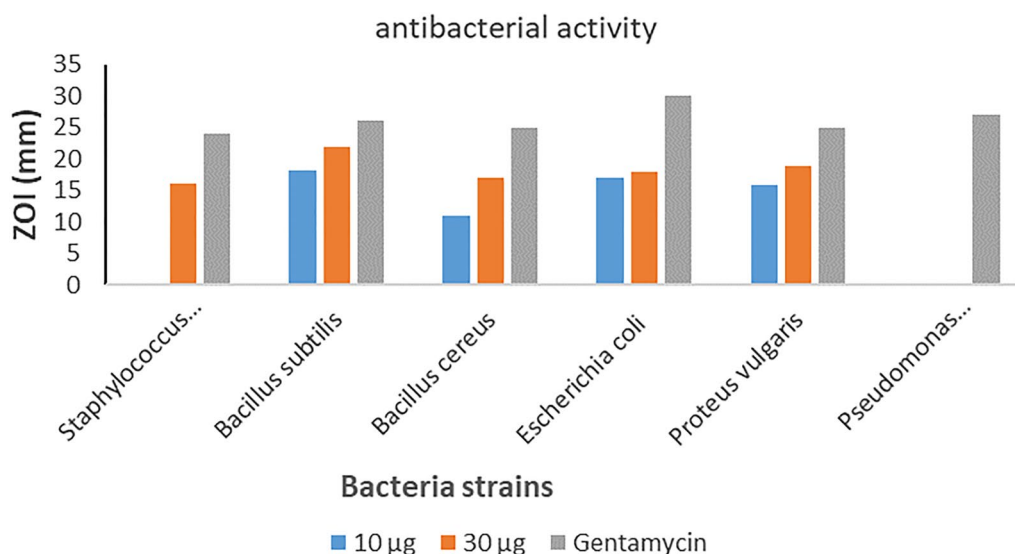


**Fig. 12** A chart depicting zones of inhibition of Cr/ZnO NPs against the test bacteria

**Table 3** Antibacterial activity of Cr/ZnO nanocomb

Inhibition zone diameter in mm Tested bacteria	Cr/ZnO (Mean ± SE)		Positive control
	10 µg	30 µg	
Gram positive bacteria			Gentamycin
<i>Staphylococcus aureus</i>	Non sensitive	16 ± 0.45	24 ± 1.07
<i>Bacillus subtilis</i>	18.13 ± 0.41	21.9 ± 0.85	26 ± 0.64
<i>Bacillus cereus</i>	11 ± 1.00	16.93 ± 0.60	25 ± 1.04
Gram negative bacteria			
<i>Escherichia coli</i>	16.96 ± 0.25	17.93 ± 0.60	30 ± 0.20
<i>Proteus vulgaris</i>	15.96 ± 0.45	19 ± 1.00	25 ± 1.09
<i>Pseudomonas aeruginosa</i>	Non sensitive	Non sensitive	27 ± 0.86

Besides, a strong absorption edge was detected at 390 nm attributed to electron transition from valence band (V.B) to conduction band (C.B), Fig. 4a. The optical reflectance displayed peaks and valleys ascribed to electron-photon interaction or electron scattering, Fig. 4b [36, 37]. The optical absorption coefficient ( $\alpha$ ) was calculated from T% and R% using the following relation:

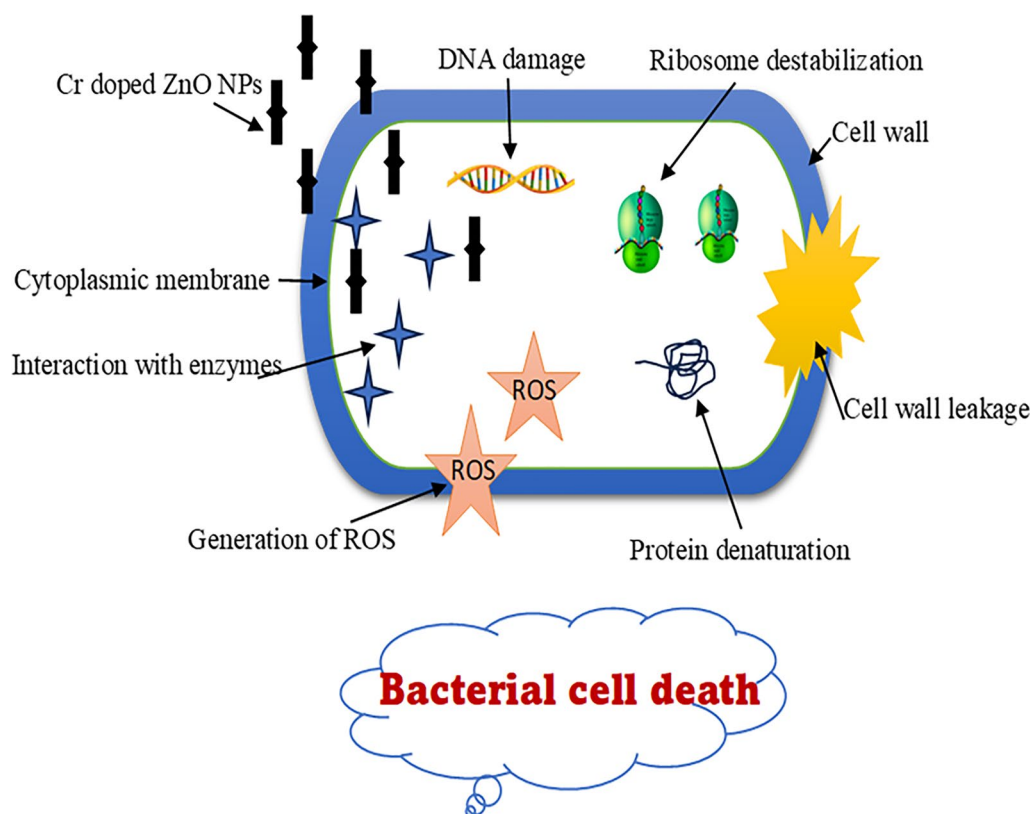
$$\alpha = \frac{1}{d} \ln \left[ \frac{(1 - R^2)}{2T} + \sqrt{\frac{(1 - R)}{4T^2} + R^2} \right] \quad (4)$$

Figure 5a illustrates the absorption coefficient as a function of photon energy ( $h\nu$ ). The thin film exhibits an optical absorption peak at  $\sim 3.20$  eV in which the electron absorbs incident photon energy and jumps to the conduction band leading to increased free charge carriers

[36]. For further optical analysis, the optical band gap ( $E_g$ ) was determined from Tauc's equation expressed as [37]:

$$\alpha = \frac{A}{h\nu} (h\nu - E_g)^n \quad (5)$$

Here, A is an independent constant, and n is constant value determines the electron transition behavior. here, n was taken by the value 0.5 refers to allowed direct transition. The  $E_g$  of Cr doped ZnO was evaluated from  $(\alpha h\nu)^2$  versus  $(h\nu)$  plot by extending the straight part to zero photon energy axis equals 3.31 eV, Fig. 5b. The wide energy gap emphasizes the quantum size effect of the nanocomposite which is attributed to the large surface area and reactive surface sites [37, 38]. Cr/ZnO nanocombs show a wide energy gap that is attributed to the small particle size. The substitution of Cr in the host lattice results in broadening of the energy gap, which also



**Fig. 13** Antibacterial activity mechanism of Cr/ZnO NPs

generates more free charge carriers according to Moss-Burstein effect. Both reactive oxygen species (ROS) in addition to metal ions production have a strong impact on harmful internal components comprising proteins and DNA causing bacterial and larvicidal death [39].

#### Mosquito larvicidal activity

Different concentrations of Cr/ZnO nanocomb were applied on the third larval instars of *C. pipiens* for 24 h to evaluate their efficacy. The findings refer to an increase in nanoparticle concentrations leading to high larval mortality. As presented in Table 2, the death rate was 100% at the ratio of 200 ppm and  $35 \pm 0.629\%$  at 25 ppm. The  $LC_{50}$  and  $LC_{90}$  values were 30.15 and 100.22 ppm, respectively while the control did not show any toxicity to mosquito larvae and Chi-square ( $\chi^2$ ) value shows a significant difference at  $p < 0.01$  level. The probability analysis of *C. pipiens* larval mortality utilizing the nanocomposites was shown in Fig. 6. The results of this work indicated the mortality of mosquito larvae caused by the internal toxic power of small particles inside the cuticle and the accumulation of nanoparticles in the alimentary canal particularly in the midgut which represents a defense region against the

toxicity of insecticides. Also, comb and needle particles can penetrate the larval midgut, damaging DNA, overlapping with organelles, and interrupting physiological processes, which prevent mosquito larvae growth and cause death [40, 41]. Related results were reported by Gunathilaka et al. and Ibrahim and Ali, ZnO NPs were effective against mosquito larvae caused mortality to the first larval instar of *C. pipiens* and star-shaped ZnO NPs were more effective against larvae than needle, round, and cubical-shapes [42, 43]. Moreover, metal and metal oxide nanoparticles have strong toxicity and physiological impact on insect pests [43–45].

#### Light and SEM images

The synthesized Cr/ZnO nanoparticles impacting *C. pipiens* larvae caused a change in their morphology features as indicated by histopathological studies after 48 h of treatment, as illustrated in (Figs. 7, 8). Light microscope images of treated larvae with fabricated samples showed the deformation in head and abdominal segments with an accumulation of nanoparticles in the alimentary canal (Fig. 7b, c) compared with the normal structure of the controlled one (Fig. 7a). Moreover,

SEM microscopy images of the control larval instar observed normal morphological structures of the head and abdominal structure without any malformation (Fig. 8a, c), while (Fig. 8b, d) illustrated the destroyed head and mouth parts and deformation of the abdominal segments. This observation is similar to the works of literature [46, 47].

#### Ultrastructural changes in the midgut of *C. pipiens* larvae by Cr/ZnO treatment

Transmission electron micrographs of the midgut of control and LC<sub>50</sub> treated *C. pipiens* larvae illustrated how the particles interact with the larval body cells compared to the control larvae. The ultrastructure of the normal epithelial cell of *C. pipiens* larvae midgut has uniform microvilli, and the nucleus with scattered chromatin (Fig. 9a, b) was depicted previously by literature [48]. The cytoplasm of the control larvae showed regular structure and normal distribution of the cell organelles and normal nuclei are central and rounded as shown in (Fig. 9c, d). Conversely, Cr/ZnO nanocomb treated midgut epithelial cells display complete destruction and rupture near the basement membrane. There was a clear abnormal nuclei shape with heterochromatin and the aggregation of a high amount of needle-shape nanocomposites in the cytoplasm destroyed cell structure and entered the hemocoel resulting in insect death. (Fig. 10a, b, c). Moreover, the treated larvae showed several forms of vacuolation in the cytoplasm, and a clear condensation appeared in the nucleus and vacuolated nuclei (Fig. 10d, e, f). Similar changes have been reported by Ibrahim et al. about the abnormal appearance of the midgut epithelia as condensation of the nuclear chromatin, abnormal shape of nuclei, absence of microvilli, and appearance of numerous vacuoles of *C. pipiens* immature stages exposed to ZnO NPs [49]. The gut in insects has a key role in regulating different mechanisms as a vital organ in ecotoxicological investigations since the epithelial midgut is the first organ exposed to a large amount of toxins ingested by an insect [50]. Additionally, the midgut represented a physical and chemical barrier to toxic substances ingested during feeding and ZnO NPs treated larvae showed that the microvilli of the midgut cells lining were very short compared to control as well as many vacuolations appeared in the cytoplasm and a clear condensation appeared in the nucleus [51]. Mohamed et al. reported that MnCoO nanostructures induce significant damage in the midgut structure of *C. pipiens* which showed the destruction of columnar epithelial cells causing the widening of intercellular spaces, and cytoplasmic vacuolization [52]. The mode action of metal oxide nanoparticles in the larval midgut via its influence on digestive tract enzymes, DNA malformation, production of reactive oxygen species,

causing cellular leakage, and disorder of the organelle functions causing larval death [53].

#### Antimicrobial activity

Antimicrobial results revealed that the Cr doped zinc oxide nanoparticles are more efficient against pathogenic bacteria at high concentrations. As shown in (Fig. 11, 12) and Table 3, *Bacillus subtilis* was the most sensitive among the tested microbes with 21.9 mm inhibition zone at 30 µg. Moreover, the inhibition zones of *Staphylococcus aureus* and *Bacillus cereus* were 16 and 16.93 mm, respectively at the high concentration. *Escherichia coli* and *Proteus vulgaris* have an inhibition zone of 17.93 and 19 mm, respectively while *Pseudomonas aeruginosa* showed non sensitivity at the same concentration. However, the control drug exhibited higher activity compared to Cr/ZnO nanocomb as demonstrated in the Table 3. From the results, the antibacterial activity of the nanoparticles was concentration dependent. The comb shape of Cr doped ZnO increased the penetration and harmed both gram-positive and gram-negative bacteria as the needles produced from it enhanced the potential activity of nanocomposite in destroying the pathogenic bacteria although most bacterial structures are resistant to major antibiotics. Besides that, Gram-negative bacteria have a great attraction towards positively charged nanoparticles, which result in cellular destruction [54]. In the present work, the antimicrobial activity of the nanocomb is efficacious against pathogenic microorganisms. These findings agree with earlier studies that demonstrated the antibacterial potential of Cr doped ZnO nanostructure against pathogenic gram-positive and gram-negative bacteria such as *Escherichia coli*, *Staphylococcus aureus*, *Pseudomonas aeruginosa*, and *Bacillus cereus* [55, 56]. Also, Vijayalakshmi and Sivaraj investigated the antibacterial activity of Cr doped ZnO nanocomb results indicated enhanced bactericidal activities against *E. coli* and *S. aureus* compared to undoped ZnO-NPs [57]. The enhanced bactericidal activity of Cr-doped ZnO was associated with an increase in ROS production, and a reduction in particle size [58, 59].

Furthermore, the mechanisms of metal oxide nanomaterials as anti-bacterial agents show through interrupting the microbial cell directly or producing reactive oxygen species (ROS) that cause DNA damage, lipid peroxidation, and protein oxidation, also can destroy bacterial cells via the penetration and leakage of the bacterial membranes [60–62]. These intracellular functional disorders are initiated by the oxidative stress manipulated by ROS leading to cell death as illustrated in Fig. 13 according to Shah et al. [54, 60]. These results coincided with Olejnik et al. (2021) who reported that the ZnO nanocomb recorded higher

toxicity as compared with spherical particles underlining the significance of particle size and shape for cytotoxicity [63]. Also, Babayevska et al. (2022) have shown that zinc oxide rods have the ability to penetrate through bacteria more easily than spheres [64]. Moreover, the Cr doped ZnO provides a more effective anti-bacterial agent compared to the pristine ZnO [57].

## Conclusions

Cr doped ZnO nanocomposite was successfully synthesized by simple co-precipitation method. The prepared sample was characterized using various spectroscopic techniques suggesting small crystallite size, large internal strain, and dislocation density of  $\sim 36 \times 10^{-4} \text{nm}^{-2}$ . Integration of  $\text{Cr}^{3+}$  inside the host ZnO matrix was confirmed using EDX and FTIR spectra. The SEM images revealed the nanocomb structure of Cr/ZnO with aspect ratio = 13 and large surface area. Moreover, the TEM image showed the particles in nanoflakes linked with sharp needles. The morphological analysis emphasized the special shape and structure of the nanocomposite which can enable it to be used as an efficient larvicidal and anti-bacterial agent. The fabricated thin film exhibited a wide band gap of 3.31 eV close to the visible region. In larvicidal study, the nanoparticles result in 100% mortality at concentration 200 ppm beside that the treated larvae showed destruction in midgut epithelium cells and malformation of their organelles. In antimicrobial activity, the nanocomb strongly caused DNA damage to bacterial cells and cell membrane leakage which results in cell death. In conclusion, the synthesized Cr/ZnO nanocomposite exhibited a significant impact on eradicating microbes and mosquitoes anchored to their superior structural-morphological and optical characteristics.

## Abbreviations

NPs	Nanoparticles
XRD	X-ray diffraction
EDX	Energy dispersive X-ray spectroscopy
FTIR	Fourier-transform infrared spectroscopy
SEM	Scane electron microscopy
TEM	Transmission electron microscopy
Abd	Abdomen
G	Gills
H	Head
Siph	Siphon
Th	Thorax
dAbd	Deformed abdomen
dH	Deformed head
Mp	Mouthparts
Cy	Cytoplasm
M	Mitochondria
N	Nucleus
Ne	Nuclear envelope
MV	Microvilli.
Nu	Nucleus

Ch	Chromatin clumps
dMV	Microvilli
HC	Heterochromatin
Ab N	Abnormal nucleus
VN	Vacuole nucleus

## Author contributions

EE raising the idea, nanomaterials synthesis and physical characterization, and writing the original draft. WAM supervised the biological tests. SAE performed the biological tests and wrote the manuscript. KDO and MK revised the manuscript and supervised the research. EE and WAM reviewed the manuscript. All authors read and approved the final manuscript.

## Funding

Open access funding is provided by The Science, Technology & Innovation Funding Authority (STDF) in cooperation with The Egyptian Knowledge Bank (EKB). This work was supported by funds from Zagazig University, Egypt.

## Availability of data and materials

The datasets used and/or analyzed during the current study are available from the corresponding author on reasonable request.

## Declarations

### Ethics approval and consent to participate

Not applicable.

### Consent for publication

Not applicable.

### Competing interests

The authors declare that they have no competing interests.

Received: 21 October 2023 Accepted: 21 December 2023

Published online: 12 January 2024

## References

- Mojahed N, Mohammadkhani MA, Mohammadkhani A. Climate crises and developing vector-borne diseases: a narrative review. *Iran J Public Health*. 2022;51:2664–73.
- Asad H, Carpenter DO. Effects of climate change on the spread of Zika Virus: a public health threat. *Rev Environ Health*. 2018;33:31–42.
- Diner RE, Kaul D, Rabines A, Zheng H, Steele JA, Griffith JF, Allen AE. Pathogenic vibrio species are associated with distinct environmental niches and planktonic taxa in southern california (usa) aquatic microbiomes. *mSystems*. 2021;6:e00571–21.
- Leibovici DG, Bylund H, Bjorkman C, Tokarevich N, Thierfelder T, Evengard B, Quegan S. Associating land cover changes with patterns of incidences of climate-sensitive infections: an example on tick-borne diseases in the nordic area. *Int J Environ Res Public Health*. 2021;20:10963.
- World Health Organization (WHO). Dengue and severe dengue. 2022; <https://www.who.int/news-room/fact-sheets/detail/dengue-and-severe-dengue>.
- Rashed SS, Beall GW, Rashad EM, Mostafa WA. Control of human filarial vector, *C. quinquefasciatus* (Diptera: *Cuicidae*) through combination of the entomopathogenic fungus, *Metarhizium anisopliae* and nanoparticles of zinc oxide and aluminum oxide. *J Egypt Soc Parasitol (JESP)*. 2020;50(1):221–7.
- Aziz A, Alshehri MA, Alanazi NA, Panneerselvam C, Trivedi S, Maggi F, Sut S, Dall'Acqua S. Phytochemical analysis of *Rhazya stricta* extract and its use in fabrication of silver nanoparticles effective against mosquito vectors and microbial pathogens. *Sci Total Environ*. 2020;700:134443.
- Khana ST, Musarrat J, Al-Khedhairi AA. Countering drug resistance, infectious diseases, and sepsis using metal and metal oxides nanoparticles: Current status. *Colloids Surf, B*. 2016;146:70–83.

9. Lalabadi MA, Hashemi H, Feng J, Jafari SM. Carbon nanomaterials against pathogens; the antimicrobial activity of carbon nanotubes, graphene/graphene oxide, fullerenes, and their nanocomposites. *Adva in Colloid and Interface Sci.* 2020;284: 102250.
10. Mondal A, Umekar MS, Bhusari GS, Chouke PB, Lambat T, Mondal S, Chaudhary RG, Mahmood SH. Biogenic synthesis of metal/metal oxide nanostructured materials. *Curr Pharm Biotechnol.* 2021;22:1782–93.
11. Abdel-Raouf AM, Osman AOE, El-Desouky EA, Abdel-Fattah A, Abdul-Kareema RF, Elgazzar E. Fabrication of an (a-Mn<sub>2</sub>O<sub>3</sub>:Co)-decorated CNT highly sensitive screen printed electrode for the optimization and electrochemical determination of cyclobenzaprine hydrochloride using response surface methodology. *RSC Adv.* 2020;10:24985.
12. Han W, Xiang W, Meng Z, Dong S, Ying L. A novel Cr-doped CdS/ZnO nanocomposite for efficient photocatalytic hydroxylation of benzene to phenol. *Coll Surfaces A Physicochem Engin Aspects.* 2023;670:131529.
13. Umashankar R, Devi SH, Gurushantha K, Manjunatha SO, Al-Dossari M, Shobha G, Kumar KJ, Kumar MR, Keshavamurthy K, NS EL-Gawaad, Madhu A, Reddy SS, Srinatha N. Improved photocatalytic, antimicrobial and photoelectrochemical properties of nanocrystalline Cu<sup>2+</sup>-doped ZnO nanoparticles. *Ceramics Intern.* 2023;49:22449–59.
14. Mirzapoor A, Ghashghaee E. Nano engineered synthesis layer by layer and transparent synergistic antimicrobial coating based on Se/Ag/TiO<sub>2</sub>/ZnO hybrid nanostructures. *Inorg Chem Comm.* 2023;153: 110840.
15. Vu AT, Tuyet Pham TA. Study on method of doping au nanoparticles on ZnO stratified microstructure to enhance photocatalytic ability and antibacterial activity. *Bull of Chem Reac Engin Cata.* 2023;18:131–50.
16. El-Latef EA, Wahba MN, Mousa S, El-Bassyouni GT, El-Shamy AM. Cu-doped ZnO-nanoparticles as a novel eco-friendly insecticide for controlling *Spodoptera littoralis*. *Biocata and Agric Biotech.* 2023;52: 102823.
17. Singh J, Dotiyal M, Bhardwaj P, Kumar K, Bhandari P, Verma V. Influence of anionic surfactant (SDS) on the structural properties of chromium oxide (Cr<sub>2</sub>O<sub>3</sub>) nanoparticles. *Mater Today Proc.* 2022;69:193–8.
18. Debnath T, Chakraborty T, Bandyopadhyay A, Sharma S, Mahapatra AS, Das S, Sutradhar S. Modulation of structural, morphological and electrical charge transport property of Cr-doped ZnO nanomaterials prepared by chemical process. *Mater Sci Eng B.* 2022;280:15688.
19. Imam Shah N, Jabeen N, Irum S, Shafique Ahmad K, Tauseef I, Farooq Khan T, Anwaar S, Shafique S, Kashif Haleem S, Mehmood A, Zaheer Husain S. Environmentally benign and economical bio-fabrication of ZnO and Cr-doped ZnO nanoparticles using leaf extract of *Citrus reticulata* for biological activities. *Mat Today Commun.* 2021;27:102383.
20. Abdel-Gawad DRI, Shaban NS, Moselhy WA, El-Dek SI, Ibrahim MA, Azab AA, NEL-Houda, Y. Hassan,. Estimating the in vitro cytotoxicity of the newly emerged zinc oxide (ZnO) doped chromium nanoparticles using the human fetal lung fibroblast cells (WI38 cells). *J Trace Elem Med Biol.* 2024;81:127342.
21. Panchal P, Sharma R, Reddy AS, Nehra K, Sharma A, Nehra SP. Eco-friendly synthesis of Ag-doped ZnO/MgO as a potential photocatalyst for antimicrobial and dye degradation applications. *Coordination Chem Rev.* 2023;493: 215283.
22. Mostafa WA, Abdel-Raouf AM, Attala K, Elgazza E. Enhancement the larvicidal activity of nanostructure copper oxide against *Culex pipiens* mosquito by yttrium replacement based on crystallite size reduction and topographic surface nature. *Mater Res Express.* 2021;8: 115006.
23. El-Samad LM, Bakr NR, El-Ashram S, Radwan EH, Abdul Aziz KK, Hussein HK, El Wakil A, Hassan MA. Silver nanoparticles instigate physiological, genotoxicity, and ultrastructural anomalies in midgut tissues of beetles. *Chem Biol Interact.* 2022;367: 110166.
24. Bharathi DS, Boopathyaraja A, Nachimuthu S, Kannan K. Green synthesis, characterization and antibacterial activity of SiO<sub>2</sub>-ZnO nanocomposite by dictyota bartayresiana extract and its cytotoxic effect on HT29 cell line. *J Cluster Sci.* 2022;33:2499–515.
25. Debnath T, Chakraborty T, Bandyopadhyay A, Sharma S, Mahapatra AS, Das S, Sutradhar S. Modulation of structural, morphological and electrical charge transport property of Cr-doped ZnO nanomaterials prepared by chemical process. *Mater Sci and Engin B.* 2022;280:115688.
26. Lokesh HS, Prinsloo ARE, Mohanty P, Sheppard CJ. Impact of Cr doping on the structure, optical and magnetic properties of nanocrystalline ZnO particles. *J Alloys Comp.* 2023;960:170815.
27. Nadeem MS, Munawar T, Mukhtar F, Rahman MN, Riaz M, Iqbal F. Enhancement in the photocatalytic and antimicrobial properties of ZnO nanoparticles by structural variations and energy bandgap tuning through Fe and Co co-doping. *Ceramics Inter.* 2021;47:11109–21.
28. David SA, Doss A, Pole RPP. Biosynthesis of chromium oxide nanoparticles by *Momordica charantia* leaf extract: characterization and their antibacterial activities. *Res Surfaces Interfaces.* 2023;11: 100120.
29. Ashokkumar M, Muthusamy C. Role of ionic radii and electronegativity of co-dopants (Co, Ni and Cr) on properties of Cu doped ZnO and evaluation of In-vitro cytotoxicity. *Surfaces Interfaces.* 2022;30: 101968.
30. Mathai J, Jose AK, Anjana MP, Aleena PA, Kunjumon J, Ittyachan R, Nair SS, Vinitha G, Sajana D. Substantial effect of Cr doping on the third-order nonlinear optical properties of ZnO nanostructures. *Opt Mater.* 2023;142: 114128.
31. Umashankar R, Devi SH, Gurushantha K, Manjunatha SO, Al-Dossari M, Shobha G, Kumar KJR, Kumar MRS, Keshavamurthy K, Abd EL-Gawaad NS, Madhu A, Reddy SS, Srinatha N. Improved photocatalytic, antimicrobial and photoelectrochemical properties of nanocrystalline Cu<sup>2+</sup>-doped ZnO nanoparticles. *Ceram Inter.* 2023;49:22449–59.
32. Rajivgandhi GN, Ramachandran G, Alharbi NS, Kadaikunnan S, Khaled JM, Manokaran N, Li W. Substantial effect of Cr doping on the antimicrobial activity of ZnO nanoparticles prepared by ultrasonication process. *Mate Sci and Engin B.* 2021;263: 114817.
33. Mathai J, Anjana MP, Aleena PA, Thomas SA, Jose AK, Kunjumon J, Nair SS, Isaac RS, Sajana D. Cr doped ZnO nanoparticles as photocatalyst for the degradation of methylene blue dye. *J of the Indian Chem Soc.* 2023;100: 101067.
34. Prakasam APM, Raj RA, Ragupathi C, Kumar R. Morphologies, crystal structure and antibacterial properties of chromium substituted zinc oxide nanoparticles synthesized by microwave method. *Mate Today Proc.* 2022;49:2928–33.
35. El-sayed HM, Abdel-Raouf AM, Abdellatef HE, Hendawy HAM, El-Abassy OM, Ibrahim H. Versatile eco-friendly electrochemical sensor based on chromium-doped zinc oxide nanoparticles for determination of safinamide aided by green assessment criteria. *Microchem J.* 2022;182: 107900.
36. Mary KL, Manonmoni JV, Balanc AMR, Karthik PS, Malliappan SP. Phytochemical assisted synthesis of Ni doped ZnO nanoparticles using aloe vera extract for enhanced photocatalytic and antibacterial activities. *Digest J of Nanomater and Biostruc.* 2022;17:634–48.
37. Hashem FM, Elgazzar E, Mostafa WA. Ultrastructural changes in the fat body of desert locust, *Schistocerca gregaria* (Orthoptera: Acrididae) treated with zinc chromium oxide nanostructures via chemical co-precipitation approach. *BMC Chem.* 2023;17:7.
38. Boulahlib S, Dib K, Ozacar M, Bessekhoud Y. Optical, dielectric, and transport properties of Ag-doped ZnO prepared by Aloe Vera assisted method. *Optical Mater.* 2021;113: 110889.
39. Debnath T, Chakraborty T, Bandyopadhyay A, Sharma S, Mahapatra AS, Das S, Sutradhar S. Modulation of structural, morphological and electrical charge transport property of Cr-doped ZnO nanomaterials prepared by chemical process. *Mater Sci Eng B.* 2022;280: 115688.
40. Abinaya M, Vaseeharan B, Divya M, Sharmili A, Govindarajan M, Alharbi NS, Kadaikunnan S, Khaled JM, Benelli G. Bacterial exopolysaccharide (EPS)-coated ZnO nanoparticles showed high antibiofilm activity and larvicidal toxicity against malaria and Zika virus vectors. *J Trace Elem Med Biol.* 2018;45:93–103.
41. Nivetha A, Sakthivel C, Hemalatha J, Senthil C, Prabha I. Fabrication of a bifunctionalized Calotropis gigantea inspired Ag-Cu-Co trimetal oxide for the remediation of methylene blue, and its larvicidal and antibacterial applications. *New J Chem.* 2023;47:12375–92.
42. Gunathilaka UMTM, de Silva WAPP, Dunuweera SP, Rajapakse RMG. Effect of morphology on larvicidal activity of chemically synthesized zinc oxide nanoparticles against mosquito vectors. *RSC Adv.* 2021;11:8857–66.
43. Ibrahim AMA, Ali AM. Silver and zinc oxide nanoparticles induce developmental and physiological changes in the larval and pupal stages of *Spodoptera littoralis* (Lepidoptera: Noctuidae). *J Asia Pac Entomol.* 2018;21:1373–8.
44. Athanassiou CG, Kavallieratos NG, Benelli G, Losic D, Rani UP, Desneux N. Nanoparticles for pest control: current status and future perspectives. *J Pest Sci.* 2018;91:1–15.

45. Mohamed RA, Ghazali NM, Kassem LM, Elgazzar E, Mostafa WA. Synthesis of MnCoO/CNT nanoflakes for the photocatalytic degradation of methyl orange dye and the evaluation of their activity against *Culex pipiens* larvae in the purification of fresh water. *RSC Adv.* 2022;12:29048–62.
46. Ishwarya R, Vaseeharan B, Kalyani S, Banumathi B, Govindarajan M, Alharbi NS, Kadaikunnan S, Al-anbr MN, Khaled JM, Benelli G. Facile green synthesis of zinc oxide nanoparticles using *Ulva lactuca* seaweed extract and its evaluation of photocatalytic, antibiofilm and larvicidal activity: impact on mosquito morphology and biofilm architecture. *J Photochem Photobiol.* 2017;178:249–58.
47. Benelli G. Mode of action of nanoparticles against insects *Environ. Sci Pollut Res.* 2018;25:12329–41.
48. Al-Doaiss A, Al-Mekhlafi F, Abutaha N, Al-Keridis LA, Shati AA, Al-Kahtani MA, Alfaifi MY. Morphological, histological and ultrastructural characterization of *Culex pipiens* (Diptera: Culicidae) larval midgut. *African Entomol.* 2021;29:274–88.
49. Ibrahim AM, Thabet MA, Ali AM. Physiological and developmental dysfunctions in the dengue vector *Culex pipiens* (Diptera: Culicidae) immature stages following treatment with zinc oxide nanoparticles. *Pestic Biochem Physiol.* 2023;192: 105395.
50. Polidori C, Pastor A, Jorge A, Pertusa J. Ultrastructural alterations of midgut epithelium, but not greater wing fluctuating asymmetry, in: Paper Wasps (*Polistes Dominula*) from Urban Environments. *Microscopy Microanalysis.* 2018;24:183–92.
51. Stojanovic J, Milosevic D, Vitorovic J, Savic-Zdravkovic D, Stankovic N, Stankovic J, Vasiljevic P. Histopathology of *Chironomus riparius* (Diptera, Chironomidae) exposed to metal oxide nanoparticles. *Arch Biol Sci.* 2021. <https://doi.org/10.2298/ABS210515025S>.
52. Mohamed RA, Kassem LM, Ghazali NM, Elgazzar E, Mostafa WA. Modulation of the Morphological Architecture of Mn<sub>2</sub>O<sub>3</sub> Nanoparticles to MnCoO Nanoflakes by Loading Co<sup>3+</sup> Via a Co-Precipitation Approach for Mosquitocidal Development. *Micromachines.* 2023;14(3):567.
53. Shamseldean MSM, Attia MM, Korany RMS, Othamn NA, Allam SFM. Insecticidal efficacy of nanomaterials used to control mosquito, *Culex quinquefasciatus* Say, 1823 with special reference to their hepatotoxicity in rats. 2022. *Biosci Reports.* <https://doi.org/10.1042/BSR20220630>.
54. Shah NI, Jabeen N, Irum S, Ahmad KS, Tauseef T, Khan TF, Anwaar S, Shafique S, Haleem SK, Mehmood N, Hussain SZ. Environmentally benign and economical bio-fabrication of ZnO and Cr-doped ZnO nanoparticles using leaf extract of *Citrus reticulata* for biological activities. *Mater Today Commun.* 2021;27: 102383.
55. Kannana K, Radhika D, Kasai RD, Gnanasangeetha D, Palani G, Gurushankar K, Koutavarapug R, Lee D, Shim J. Facile fabrication of novel ceria-based nanocomposite (CYO-CSO) via co-precipitation: electrochemical, photocatalytic and antibacterial performances. *J Mol Struct.* 2022;1256: 132519.
56. Hussain A, Oves M, Alajmi MF, Hussain I, Amir S, Ahmed J, Rehman MT, El-Seedif HR, Ali I. Biogenesis of ZnO nanoparticles using *Pandanus odorifer* leaf extract: anticancer and antimicrobial activities. *RSC Adv.* 2019;9(27):15357–69.
57. Vijayalakshmi K, Sivaraj D. Enhanced antibacterial activity of Cr doped ZnO nanorods synthesized using microwave processing. *RSC Adv.* 2015;5:68461.
58. Khalid A, Ahmad P, Alharthi AI, Muhammad S, Khandaker MU, Faruque MRI, et al. Synergistic effects of Cu-doped ZnO nanoantibiotic against Gram-positive bacterial strains. *PLoS ONE.* 2021;16: e0251082.
59. Kannan KR, Adhika D, Gnanasangeetha D, Lakkaboyana SK, Sadasivuni KK, Gurushankar K, Hanafiah MM. Photocatalytic and antimicrobial properties of microwave synthesized mixed metal oxide nanocomposite. *Inorganic Chem Commun.* 2021;125: 108429.
60. Elgazzar E, Ayoub HA, El-Wahab ZA, Mostafa WA. Integration of ZnO nanorods with silver ions by a facile co-precipitation for antimicrobial, larvicidal, and ovicidal activity. *BMC Biotechnol.* 2023;23:23.
61. Lakshmanana A, Surendrana B, Priyaa SS, Balakrishnana K, Geethab P, Rameshkumara P, Hegdec TA, Vinithac G, Kannand K. Investigations on structural, optical, dielectric, electronic polarizability, Z-scan and antibacterial properties of Ni/Zn/Fe<sub>2</sub>O<sub>4</sub> nanoparticles fabricated by microwave-assisted combustion method. *J Photochem Photobiol A: Chemi.* 2020;402: 112794.
62. Kannan K, Radhika D, Nesaraj AS, Sadasivuni KK, Krishna LS. Facile synthesis of NiO-CYSO nanocomposite for photocatalytic and antibacterial applications. *Inorg Chem Commun.* 2020;122: 108307.
63. Olejnik M, Kersting M, Rosenkranz N, Loza K, Breisch M, Rostek A, Prymak O, Schurmeyer L, Westphal G, Oller MK, Bunger J, Epple M, Sengstock C. Cell-biological effects of zinc oxide spheres and rods from the nano- to the microscale at sub-toxic levels. *Cell Biol Toxicol.* 2021;37:573–93.
64. Babayevska N, Przysiecka L, Iatsunskyi I, Nowaczyk G, Jarek M, Janiszewska E, et al. ZnO size and shape effect on antibacterial activity and cytotoxicity profile. *Sci Rep.* 2022;12:8148.

## Publisher's Note

Springer Nature remains neutral with regard to jurisdictional claims in published maps and institutional affiliations.

Ready to submit your research? Choose BMC and benefit from:

- fast, convenient online submission
- thorough peer review by experienced researchers in your field
- rapid publication on acceptance
- support for research data, including large and complex data types
- gold Open Access which fosters wider collaboration and increased citations
- maximum visibility for your research: over 100M website views per year

At BMC, research is always in progress.

Learn more [biomedcentral.com/submissions](https://biomedcentral.com/submissions)

